Photoionization cross sections and oscillator strengths for oxygen ions: O I-O VII

Sultana N. Nahar
Department of Astronomy, The Ohio State University, Columbus, Ohio 43210
(Received 27 March 1998)

Ab initio close-coupling calculations are reported using the *R*-matrix method for photoionization cross sections ($\sigma_{\rm PI}$), oscillator strengths (f values), and energy levels (E) for oxygen ions: O I, O II, O III, O IV, O V, O VI, and O VII. Total, partial, and state-specific photoionization cross sections are computed and investigated in detail. Important features are found that should affect overall photoionization and recombination, especially at high temperatures and energies. Although these ions have been previously studied individually, present work aims at studying them as an isonuclear sequence and obtaining more accurate and complete results for applications. More extended eigenfunction expansions than in previous works, including $n=3$ states, show correlation effects primarily manifested as additional groups of resonances in photoionization of oxygen ions such as O VI and O VII that are of importance in extreme ultraviolet and x-ray laboratory and astrophysical plasmas. Lifetimes of excited bound states are obtained from the present oscillator strengths and compared with experiments. The computed radiative atomic parameters, energy levels, oscillator strengths, and photoionization cross sections constitute a larger dataset than the Opacity Project data [M. J. Seaton, J. Phys. B **20**, 6363 (1987)], with which comparisons are made. [S1050-2947(98)08711-3]

PACS number(s): 32.80.Fb

I. INTRODUCTION

Oxygen is an important element because of its existence in the Earth's atmosphere as well as in many astrophysical and laboratory spectra. For the analysis of the spectra and various other applications, radiative atomic quantities are required for all ionization stages. The present work reports the radiative data for energy values (E), oscillator strengths (f values), and photoionization cross sections ($\sigma_{\rm PI}$) for the oxygen ions O I–O VII. These ions were previously studied individually, along isoelectronic sequences, under the Opacity Project (OP) [1]. These studies include work on O I by Butler and Zeippen [2], on O II by Burke and Lennon [3], on O III by Luo *et al.* ([5], see also Nahar and Pradhan [6]), O IV by Fernley *et al.* [7], O V by Tully *et al.* [8], on O VI by Peach *et al.* [9], on O VII by Fernley *et al.* [10], and on O VIII by Seaton [12]. The OP close coupling calculations for the (e + ion) system limited the eigenfunction expansions to the $n=2$ states of the target ion, thereby restricting some electron correlation effects important at higher energies and for photoionization of excited states. The calculations for O VI and O VII did not include any electron-electron correlation effects. Inclusion of these effects in the present work has resulted in detailed resonance structures in the photoionization cross sections and enhancement in the background cross sections at the additional ionization thresholds in the eigenfunction expansions employed. One important high-energy feature in the cross sections is the *photoexcitation of core* (PEC), which introduces a wider resonance affecting the background considerably. The present work studies the oxygen isonuclear sequence to illustrate these features, and provides more consistent and complete data for applications, such as for determination of oxygen ionization fractions in a plasma source.

The calculations are carried out in the close-coupling (CC) approximation employing the *R*-matrix method. Partial cross sections for photoionization of the ground state of each oxygen ion, into the ground and a number of excited states of the residual ion, are also presented. A further reason for the recomputation of the radiative data for the oxygen ions in a more complete manner was to calculate the total recombination rate coefficients, $\alpha_R(T)$, for these ions employing the unified treatment [13]. The unified treatment for total recombination rate coefficients requires *partial* photoionization cross sections leaving the residual core in the ground state, rather than the *total* cross sections that are usually computed (such as in the OP work). The f values are also needed for radiative transition probabilities in the calculations for the dielectronic recombination cross sections. Hence a consistent set of radiative parameters for both the bound-bound transitions, f values, and the bound-free transitions, $\sigma_{\rm PI}$, in oxygen ions are obtained.

II. COMPUTATIONS

The theoretical details for the computations of photoionization cross sections and oscillator strengths in the close-coupling approximation employing the *R*-matrix method are given in previous papers [1,15]. Here only the computational details relevant to the present work for the radiative data of oxygen ions are described. The residual core ion, termed the ''target,'' is represented as an N-electron system. The wavefunction expansion, $\Psi(E)$, for a given symmetry, $SL\pi$, of the total $(N+1)$-electron system is represented in terms of the core or the ''target'' ion states as

$$\Psi(E)=A\sum_i \chi_i\theta_i+\sum_j c_j\Phi_j, \qquad (2.1)$$

where χ_i is the target ion wave function in a specific state $S_iL_i\pi_i$ and θ_i is the wave function for the $(N+1)$th electron in a channel labeled as $S_iL_i\pi_i k_i^2 \ell_i (SL\pi)$, k_i^2 being its energy. k_i^2 is <0 for bound states and $\geqslant 0$ for free states. Φ_j's are the bound channel wave functions of the $(N+1)$-electron

system that represents correlations not included in the first term and compensates for the orthogonality condition of the total wave function.

In principle, the first expansion of the above equation should have an infinite number of target terms, however, in reality the number is limited based on a few criteria. The target terms are selected such that electron-electron correlations effects are well represented within the energy range of consideration and the term contributions have converged. It is also important to include all the terms at all energies of interest. For example, the expansion may contain overlapping states from two different complexes, such as from $n=2$ and 3 of O II, as shown in Table I. Omission of states of the higher complex from the expansion, which was often a choice in the earlier works, would affect the results in several ways. If an omitted state is a low-lying one, $(N+1)$-electron bound states with the omitted target state can not be obtained, and the corresponding oscillator strengths for transitions involving these states will also be missing. The effect on the photoionization cross sections will be seen as missing Rydberg series of resonances belonging to the omitted state. The loss may be considerable if the omitted state is accessible via dipole allowed transition from the target ground state, which introduces the prominent PEC resonance in excited-state photoionization cross sections. The PEC resonances [16] occur when the outer electron remains a spectator while the core is excited via a dipole allowed transition. One important criterion in the choice of the eigenfunction expansions is the inclusion of PEC resonances at relatively high energies. The effect of PEC decreases at very high target energies when transition probability for the core transition reduces significantly. Present eigenfunction expansions are selected so as to optimize the inclusion of these effects. The targets in an isonuclear sequence do not show a specific order of terms as often seen in the case of the isoelectronic sequence. Thus, the number of terms and importance of complexes are different for each ion in the sequence.

The target states in the CC eigenfunction expansion for each oxygen ion employed are given in Table I. The orbital wave functions of the targets are obtained from the atomic structure calculations using the code SUPERSTRUCTURE [17]. The spectroscopic and correlation configurations and the values of the scaling parameter, $\lambda(nl)$, of the Thomas-Fermi-Dirac potential for each ion are also listed. The calculated target state energies are replaced by the observed ones, given in Table I, in the *R*-matrix computations to obtain more accurate positions for the Rydberg series of resonances. Some details of the eigenfunction expansion for each ion are discussed below.

An eigenfunction expansion of eight LS terms of O II (Table I), which includes the $3s$ orbital states $2p^2 3s(^4P,^2P)$, is employed in the computation for the radiative data of $(e+\mathrm{O\,II})\rightarrow \mathrm{O\,I}$. The $3s$ states were not included in the OP calculations by Butler and Zeippen [2] who employed an eigenfunction expansion restricted to the $n=2$ complex. The target states with the $3s$ orbital lie between the states $2s2p^4(^2D,^2S)$ and play a crucial role in terms of energy levels and resonances, especially for PEC resonances due to dipole allowed transition of the ground state, $^4S^o$ to the $3s(^4P)$ state in O II. In a recent calculations for photoionization cross sections of the 3 states of ground configuration, Bell *et al.* [18] have employed an 11-CC expansion, which includes both the ^4P states as in the present case. The three additional states they have considered are not expected to contribute significantly, as they lie high for bound-state formation and not connected to the ground state via a dipole allowed transitions, yet may provide better high energy behavior for the cross sections. For the second term of Eq. (1), which is the sum over the bound-channel wave functions, all possible combination of $(N+1)$-electron configurations up to $3p^2$ and $3d^2$ are included.

A 12-CC eigenfunction expansion is employed for the $(e+\mathrm{O\,III})\rightarrow \mathrm{O\,II}$ radiative calculations. In a previous work Burke and Lennon [3] also implemented a 12-CC expansion but did not include the $3s$ orbital, thereby missed the important $2s^2 2p 3s(^3P^o)$ state that is connected via a dipole allowed transition to the ground $2s^2 2p^2(^3P)$ state and gives rise to a PEC resonance. The bound-channel expansion of $(N+1)$-electron configurations includes all states dominated by configurations with $n=4$ orbitals up to the $4s$ and the $4p$.

For the radiative calculations for $(e+\mathrm{O\,IV})\rightarrow \mathrm{O\,III}$ a 23-CC eigenfunction expansion [20] (Table I) including orbitals up to $3d$ is chosen. The expansion in the earlier works [5,6] is limited to the target states of the $n=2$ complex. The present expansion includes 11 dipole allowed transitions of the target ground state, $2p(^2P^o)$, compared to 3 in the previous 8-CC expansion [5,6]. The bound channel expansion includes all possible $(N+1)$-electron states dominated by configurations $2p^4$, $3p^2$, and $3d^2$, i.e., configurations with up to 4 electrons in the $2p$ orbital and 2 electrons in the $3p$ and the $3d$ orbitals.

For $(e+\mathrm{O\,V})\rightarrow \mathrm{O\,IV}$ radiative data, a 12-CC eigenfunction expansion is used that includes states with target configurations including the $3d$ (given in Table I). The earlier work of Fernley *et al.* [7] considers the 6 lowest states in $n=2$ complex. However, contributions from the $n=3$ complex can be significant in the high-energy region for O IV, as we show below. Analogous to the case of O III, the bound channel expansion in Ψ includes all $(N+1)$-electron states up to configurations $2p^3$, $3s^2$, $3p^2$, and $3d^2$.

The radiative calculations for $e+\mathrm{O\,VI}\rightarrow \mathrm{O\,V}$ use a 9-CC target expansion (Table I). This is an extension of the 5-CC eigenfunction expansion used in the work by Tully *et al.* [8] by four additional states of the $n=4$ complex, up to $1s^2 4f$ and including the state $1s^2 4p(^2P^o)$ for the dipole allowed transition by the ground state $1s^2 2s(^2S)$ of O VI. For the bound channel expansion all states from configurations of $3p^2$, and $3d^2$, and those with single occupancy $4s$, $4p$, $4d$, and $4f$ orbitals are included.

Calculations for radiative data for $(e+\mathrm{O\,VII})\rightarrow \mathrm{O\,VI}$ are obtained using an 11-CC eigenfunction expansion including states up to the orbital $3d$ (Table I). In the previous OP work Peach *et al.* [9] employ a very limited 2-CC expansion. In spite of the small number of electrons, it turns to be rather difficult to carry out close-coupling *R*-matrix calculations for the He-like and H-like target ions. Numerical instabilities associated with the *R*-matrix basis functions in the inner regions could introduce unphysical oscillations in the photoionization cross sections. It is therefore required to optimize the calculations with a large *R*-matrix basis, as, for example, in the work of Ref. [14] for He-like and H-like carbon and nitrogen ions. The present work uses a basis set of 50 func-

TABLE I. The target states with their energies (in Rydberg) in the eigenfunction expansions of oxygen ions: the spectroscopic and correlation configurations, and the values of Thomas-Fermi scaling parameter $\lambda(nl)$, are as follows. O II: Spectroscopic: $2s^22p^3$, $2s2p^4$, $2s^22p^23s$. Correlation: $2s^22p^23p$, $2s^22p^23d$, $2p^5$, $2s2p^33s$, $2s2p^33p$, $2s2p^33d$. $\lambda(nl)$: 1.35(1s), 1.25(2s), 1.12(2p), 1.07(3s), 1.05(3p), 2.10(3d). O III: Spectroscopic: $2s^22p^2$, $2s2p^3$, $2s^22p3s$, $2p^4$. Correlation: $2s^23s^2$, $2s^23p^2$, $2s^23d^3$, $2s^24s^2$, $2s^24p^2$, $2s^22p3p$, $2s^22p3d$, $2s^22p4s$, $2s^22p4p$, $2s^23s3p$, $2s^23s4s$, $2s^23p3d$, $2s2p^23s$, $2s2p^23p$, $2s2p^23d$, $2p^33s$, $2p^33p$, $2p^33d$. $\lambda(nl)$: 1.47637(1s), 1.27184(2s), 1.19306(2p), 1.22385(3s), 1.32(3p), −0.96476(3d), −0.74971(4s), −0.79911(4p). O IV: Spectroscopic: $2s^22p$, $2s2p^2$, $2p^3$, $2s^23s$, $2s^23p$, $2s^23d$, $2s2p3s$, $2s2p3p$. Correlation: $2s3d^2$, $2s2p3d$, $2p^23s$, $2p^23p$, $2p^23d$. $\lambda(nl)$: 1.42496(1s),1.38027(2s),1.17735(2p),1.56085(3s),1.38926(3p),1.97512(3d). O V: Spectroscopic: $2s^2$, $2s2p$, $2p^2$, $2s3s$, $2s3p$, $2s3d$. Correlation: $2s4s$, $2s4p$, $2p3s$, $2p3p$. $\lambda(nl)$: 1.4(1s),1.4(2s),1.127(2p),1.2(3s),1.1(3p),1.1(3d), 10.6115(4s),4.37106(4p). O VI: Spectroscopic: $1s^22s$, $1s^22p$, $1s^23s$, $1s^23p$, $1s^23d$, $1s^24s$, $1s^24p$, $1s^24d$, $1s^24f$. Correlation: $1s2s^2$, $1s2p^2$, $1s3s^2$, $1s3p^2$, $1s3d^2$, $1s2s2p$, $1s2s3s$, $1s2s3p$, $1s2s3d$, $1s2p3s$, $1s2p3d$. $\lambda(nl)$: 1.30117(1s), 0.99782(2s), 0.87558(2p), 0.98747(3s), 0.86738(3p), 0.80564(3d), 0.98598(4s), 0.86603(4p), 0.79571(4d), 0.77675(4f). O VII: Spectroscopic: $1s^2$, $1s2s$, $1s2p$, $1s3s$, $1s3p$, $1s3d$. Correlation: $2s^2$, $2p^2$, $3s^2$, $3p^2$, $3d^2$, $2s2p$, $2s3s$, $2s3p$, $2s3d$, $2s4s$, $2s4p$, $2p3s$, $2p3p$, $2s3d$, $2s4s$, $2s4p$. $\lambda(nl)$: 0.991(1s), 0.991(2s), 0.776(2p), 1.16883(3s), 0.91077(3p), 1.00746(3d), −1.59699(4s), −1.61237(4p). O VIII: Spectroscopic: $1s$, $2s$, $2p$, $3s$, $3p$, $3d$, $4f$, $4d$, $4p$, $4s$. $\lambda(nl)$: 1.0(1s), 1.0(2s), 1.0(2p), 1.0(3s), 1.0(3p), 1.0(3d), 1.0(4s), 1.0(4p), 1.0(4d), 1.0(4f).

O II: Present: 8-CC, OP: 8-CC											
$2s^22p^3$	$^4S^o$	0.0	$2s^22p^3$	$^2P^o$	0.368778	$2s2p^4$	^2D	1.512628	$2s^22p^23s$	^2P	1.722373
$2s^22p^3$	$^2D^o$	0.244389	$2s2p^4$	^4P	1.092906	$2s^22p^23s$	^4P	1.689510	$2s2p^4$	^2S	1.783445
O III: Present: 12-CC, OP: 12-CC											
$2s^22p^2$	^3P	0.0	$2s2p^3$	$^5S^o$	0.549724	$2s2p^3$	$^1D^o$	1.704520	$2s^22p3s$	$^3P^o$	2.437687
$2s^22p^2$	^1D	0.184723	$2s2p^3$	$^3D^o$	1.093895	$2s2p^3$	$^3S^o$	1.795986	$2s^22p3s$	$^1P^o$	2.488489
$2s^22p^2$	^1S	0.393517	$2s2p^3$	$^3P^o$	1.297496	$2s2p^3$	$^1P^o$	1.917839	$2p^4$	^3P	2.586781
O IV: Present: 23-CC, OP: 8-CC											
$2s^22p$	$^2P^o$	0.0	$2p^3$	$^2D^o$	2.32300	$2s2p3s$	$^4P^o$	4.12790	$2s2p3p$	^2S	4.49155
$2s2p^2$	^4P	0.64820	$2p^3$	$^2P^o$	2.63150	$2s2p3p$	^2P	4.26769	$2s2p3s$	$^2P^o$	4.72663
$2s2p^2$	^2D	1.15678	$2s^23s$	^2S	3.25882	$2s2p3p$	^4D	4.26769	$2s2p3p$	^2D	5.05265
$2s2p^2$	^2S	1.49782	$2s^23p$	$^2P^o$	3.55594	$2s2p3p$	^4S	4.39977	$2s2p3p$	^2P	5.05265
$2s2p^2$	^2P	1.64614	$2s^23d$	^2D	3.82317	$2s2p3p$	^4P	4.39977	$2s2p3p$	^2S	5.05265
$2p^3$	$^4S^o$	2.10520	$2s2p3s$	$^4P^o$	3.99886	$2s2p3p$	^2D	4.39977			
O V: Present: 12-CC, OP: 6-CC											
$2s^2$	^1S	0.0	$2p^2$	^3P	1.94780	$2s3s$	^1S	4.98435	$2s3p$	$^3P^o$	5.29286
$2s2p$	$^3P^o$	0.74934	$2p^2$	^1D	2.11160	$2s3s$	^3S	5.11472	$2s3d$	^3D	5.47455
$2s2p$	$^1P^o$	1.44707	$2p^2$	^1S	2.62363	$2s3p$	$^1P^o$	5.29286	$2s3d$	^1D	5.58256
O VI: Present: 9-CC, OP: 5-CC											
$1s^22s$	^2S	0.0	$1s^23p$	$^2P^o$	6.07102	$1s^24s$	^2S	7.86766	$1s^24d$	^2D	7.90144
$1s^22p$	$^2P^o$	0.88146	$1s^23d$	^2D	6.14792	$1s^24p$	$^2P^o$	7.86766	$1s^24f$	$^2F^o$	7.90144
$1s^23s$	^2S	5.83247									
O VII: Present: 11-CC, OP: 2-CC											
$1s^2$	^1S	0.0	$1s2s$	^1S	41.812401	$1s3s$	^1S	48.804463	$1s3d$	^1D	48.921834
$1s2s$	^3S	41.231559	$1s2p$	$^1P^o$	42.184389	$1s3p$	$^3P^o$	48.804463	$1s3p$	$^1P^o$	48.921834
$1s2p$	$^3P^o$	41.790521	$1s3s$	^3S	48.650915	$1s3d$	^3D	48.921834			
O VIII: Present: 10-CC, OP: 1-CC											
$1s$	^2S	0.0	$3s$	^2S	56.8889	$4f$	$^2F^o$	60.00	$4s$	^2S	60.00
$2s$	^2S	48.0	$3p$	$^2P^o$	56.8889	$4d$	^2D	60.00			
$2p$	$^2P^o$	48.0	$3d$	^2D	56.8889	$4p$	$^2P^o$	60.00			

tions in the inner region encompassed by the *R*-matrix boundary, which involves considerable memory and CPU requirements. The bound channel expansion of O VI includes all states corresponding to configurations up to $3p^2$, $3d^2$, $4s$, and $4p$.

Finally, a 10-CC eigenfunction expansion is used for the radiative data calculations for $(e+\text{O VIII})\rightarrow\text{O VII}$. The expansion includes three $^2P^o$ states ($2p$, $3p$, and $4p$) enabling dipole allowed transitions from the target gound state ^2S. The earlier calculations of Fernley *et al.* [10] employ a

TABLE II. Comparison of the present calculated energies, $E(P)$, with the measured $E(\text{obs})$ values (Ref. [21] for all ions except O II for which the reference is [22]) and of the calculated values under the OP, $E(\text{OP})$, of first 20 bound states of oxygen ions. Energies are expressed in Rydberg units and negative signs are omitted for convenience. N_b is the total number of bound states below the ionization threshold obtained in this work and under the OP.

Term	$E(\text{obs})$	$E(P)$	$E(\text{OP})$	Term	$E(\text{obs})$	$E(P)$	$E(\text{OP})$
O I: $N_b=107$ (present), 69 (OP)							
$2s^22p^4(^3P)$	1.00020	0.9912	1.004	$2s^22p^3\ ^4S^o3d(^3D^o)$	0.11253	0.1122	0.1115
$2s^22p^4(^1D)$	0.85631	0.8170	0.8515	$2s^22p^3\ ^4S^o4p(^5P)$	0.09790	0.09768	0.09702
$2s^22p^4(^1S)$	0.69297	0.6634	0.6776	$2s^22p^3\ ^4S^o4p(^3P)$	0.09255	0.09186	0.09151
$2s^22p^3\ ^4S^o3s(^5S^o)$	0.32868	0.3330	0.3216	$2s^22p^3\ ^2D^o3s(^3D^o)$	0.07922	0.05710	0.07009
$2s^22p^3\ ^4S^o3s(^3S^o)$	0.30110	0.3056	0.2939	$2s^22p^3\ ^4S^o5s(^5S^o)$	0.07035	0.07001	0.6976
$2s^22p^3\ ^4S^o3p(^5P)$	0.21149	0.2126	0.2082	$2s^22p^3\ ^4S^o5s(^3S^o)$	0.06766	0.06735	0.06700
$2s^22p^3\ ^4S^o3p(^3P)$	0.19324	0.1925	0.1900	$2s^22p^3\ ^2D^o3s(^1D^o)$	0.06538	0.04455	0.05615
$2s^22p^3\ ^4S^o4s(^5S^o)$	0.13086	0.1301	0.1293	$2s^22p^3\ ^4S^o4d(^5D^o)$	0.06353	0.06370	0.06314
$2s^22p^3\ ^4S^o4s(^3S^o)$	0.12404	0.1234	0.1224	$2s^22p^3\ ^4S^o4d(^3D^o)$	0.06314	0.06312	0.06263
$2s^22p^3\ ^4S^o3d(^5D^o)$	0.11315	0.1136	0.1122	$2s^22p^3\ ^4S^o4f(^5F)$	0.06259	0.06254	0.06251
O II: $N_b=296$ (present), 219 (OP)							
$2s^22p^3(^4S^o)$	2.5814	2.597	2.604	$2s^22p^2(^1D)3s(^2D)$	0.6953	0.6716	0.6751
$2s^22p^3(^2D^o)$	2.3370	2.339	2.349	$2s^22p^2(^3P)3p(^4P^o)$	0.6820	0.6804	0.6787
$2s^22p^3(^2P^o)$	2.2126	2.208	2.217	$2s^22p^2(^3P)3p(^2D^o)$	0.6528	0.6495	0.6489
$2s2p^4(^4P)$	1.4884	1.500	1.515	$2s^22p^2(^3P)3p(^4S^o)$	0.6480	0.6462	0.6443
$2s2p^4(^2D)$	1.0687	1.054	1.075	$2s2p^4(^2P)$	0.6435	0.6178	0.6321
$2s^22p^2(^3P)3s(^4P)$	0.8918	0.8872	0.8867	$2s^22p^2(^3P)3p(^2P^o)$	0.6293	0.6245	0.6242
$2s^22p^2(^3P)3s(^2P)$	0.8590	0.8544	0.8535	$2s^22p^2(^1D)3p(^2F^o)$	0.4969	0.4770	0.4892
$2s2p^4(^2S)$	0.7979	0.7645	0.7843	$2s^22p^2(^1D)3p(^2D^o)$	0.4858	0.4675	0.4782
$2s^22p^2(^3P)3p(^2S^o)$	0.7229	0.7220	0.7210	$2s^22p^2(^1S)3s(^2S)$	0.4799	0.4216	0.4400
$2s^22p^2(^3P)3p(^4D^o)$	0.6960	0.6952	0.6936	$2s^22p^2(^3P)3d(^4F)$	0.4724	0.4672	0.4697
O III: $N_b=296$ (present), 267 (OP)							
$2s^22p^2(^3P)$	4.0358	4.066	4.037	$2s^22p(^2P^o)3s(^1P^o)$	1.5492	1.572	1.542
$2s^22p^2(^1D)$	3.8530	3.875	3.847	$2p^4(^3P)$	1.4509	1.422	1.444
$2s^22p^2(^1S)$	3.6442	3.639	3.626	$2S^22p(^2P^o)3p(^1P)$	1.3863	1.428	1.384
$2s2p^3(^5S^o)$	3.4880	3.522	3.508	$2s^22p(^2P^o)3p(^3D)$	1.3579	1.398	1.355
$2s2p^3(^3D^o)$	2.9438	2.958	2.945	$2s^22p(^2P^o)3p(^3S)$	1.3262	1.366	1.322
$2s2p^3(^3P^o)$	2.7402	2.726	2.731	$2p^4(^1D)$	1.3195	1.287	1.307
$2s2p^3(^1D^o)$	2.3332	2.322	2.312	$2s^22p(^2P^o)3p(^3P)$	1.3005	1.337	1.298
$2s2p^3(^3S^o)$	2.2417	2.220	2.216	$2s^22p(^2P^o)3p(^1D)$	1.2439	1.273	1.238
$2s2p^3(^1P^o)$	2.1199	2.081	2.087	$2s^22p(^2P^o)3p(^1S)$	1.1781	1.203	1.169
$2s^22p(^2P^o)3s(^3P^o)$	1.6000	1.635	1.596	$2s2p^2(^4P)4p(^3S^o)$	0.0553	0.06102	0.07502
O IV: $N_b=109$ (present), 94 (OP)							
$2s^22p(^2P^o)$	5.6875	5.674	5.674	$2s^23d(^2D)$	1.8666	1.868	1.861
$2s2p^2(^4P)$	5.0370	5.031	5.031	$2s2p(^3P^o)3s(^4P^o)$	1.6886	1.687	1.684
$2s2p^2(^2D)$	4.5330	4.507	4.514	$2s2p(^3P^o)3s(^2P^o)$	1.5619	1.555	1.552
$2s2p^2(^2S)$	4.1920	4.134	4.159	$2s2p(^3P^o)3p(^2P)$	1.4314	1.428	1.429
$2s2p^2(^2P)$	4.0437	4.001	4.014	$2s2p(^3P^o)3p(^4D)$	1.4197	1.417	1.417
$2p^3(^4S^o)$	3.5799	3.539	3.563	$2s2p(^3P^o)3p(^4S)$	1.3660	1.363	1.360
$2p^3(^2D^o)$	3.3645	3.320	3.344	$2s2p(^3P^o)3p(^4P)$	1.3249	1.320	1.320
$2p^3(^2P^o)$	3.0560	2.975	3.023	$2s2p(^3P^o)3p(^2D)$	1.2900	1.282	1.282
$2s^23s(^2S)$	2.4310	2.431	2.424	$2s^24s(^2S)$	1.2627	1.261	1.260
$2s^23p(^2P^o)$	2.1339	2.135	2.129	$2s2p(^3P^o)3p(^2S)$	1.1982	1.184	1.183

TABLE II. (*Continued*).

Term	E(obs)	$E(P)$	E(OP)	Term	E(obs)	$E(P)$	E(OP)
O V: $N_b=152$ (present), 120 (OP)							
$2s^2(^1S)$	8.3714	8.357	8.357	$2s3d(^3D)$	2.8969	2.894	2.895
$2s2p(^3P^o)$	7.6221	7.608	7.609	$2s3d(^1D)$	2.7889	2.782	2.783
$2s2p(^1P^o)$	6.9243	6.892	6.891	$2p3s(^3P^o)$	2.4186	2.412	2.413
$2p^2(^3P)$	6.4236	6.398	6.398	$2p3s(^1P^o)$	2.3162	2.306	2.307
$2p^2(^1D)$	6.2598	6.233	6.232	$2p3p(^1P)$	2.2414	2.234	2.236
$2p^2(^1S)$	5.7478	5.689	5.682	$2p3p(^3D)$	2.1980	2.191	2.192
$2s3s(^3S)$	3.3871	3.382	3.383	$2p3p(^3S)$	2.1389	2.131	2.132
$2s3s(^1S)$	3.2567	3.251	3.251	$2p3p(^3P)$	2.0873	2.076	2.077
$2s3p(^1P^o)$	3.0786	3.073	3.074	$2p3d(^3F^o)$	2.0576	2.054	2.055
$2s3p(^3P^o)$	3.0598	3.054	3.055	$2p3d(^1D^o)$	2.0414	2.037	2.037
O VI: $N_b=51$ (present), 26 (OP)							
$1s^22s(^2S)$	10.1516	10.14	10.14	$1s^25p(^2P^o)$	1.4574	1.457	1.457
$1s^22p(^2P^o)$	9.2701	9.264	9.263	$1s^25d(^2D)$	1.4412	1.441	1.441
$1s^23s(^2S)$	4.3191	4.318	4.316	$1s^25f(^2F^o)$	1.4401	1.440	
$1s^23p(^2P^o)$	4.0806	4.081	4.078	$1s^25g(^2G)$	1.4400	1.440	
$1s^23d(^2D)$	4.0037	4.007	4.003	$1s^26s(^2S)$	1.0382	1.038	1.038
$1s^24s(^2S)$	2.3812	2.380	2.380	$1s^26p(^2P^o)$	1.0104	1.010	1.010
$1s^24p(^2P^o)$	2.2839	2.283	2.283	$1s^26d(^2D)$	1.0008	1.001	1.001
$1s^24d(^2D)$	2.2519	2.252	2.252	$1s^26f(^2F^o)$	1.0000	1.000	
$1s^24f(^2F^o)$	2.2501	2.250		$1s^26g(^2G)$	1.0000	1.000	
$1s^25s(^2S)$	1.5065	1.505	1.506	$1s^26h(^2H^o)$	0.9999	1.000	
O VII: $N_b=105$ (present), 53 (OP)							
$1s^2(^1S)$	54.340	54.25	54.27	$1s3p(^1P^o)$	5.418	5.417	5.418
$1s2s(^3S)$	13.108	13.09	13.09	$1s4s(^3S)$	3.160	3.158	3.158
$1s2p(^3P^o)$	12.549	12.54	12.54	$1s4p(^3P^o)$	3.099	3.096	3.097
$1s2s(^1S)$	12.527	12.51	12.51	$1s4s(^1S)$	3.098	3.096	3.096
$1s2p(^1P^o)$	12.156	12.14	12.15	$1s4d(^3D)$	3.070	3.064	3.064
$1s3s(^3S)$	5.689	5.677	5.677	$1s4f(^3F^o)$	3.070	3.063	
$1s3p(^3P^o)$	5.535	5.526	5.527	$1s4d(^1D)$	3.066	3.062	3.062
$1s3s(^1S)$	5.529	5.522	5.523	$1s4f(^1F^o)$	3.064	3.063	
$1s3d(^3D)$	5.456	5.448	5.448	$1s4p(^1P^o)$	3.053	3.051	3.052
$1s3d(^1D)$	5.446	5.444	5.444	$1s5s(^3S)$	2.009	2.008	2.008

5-CC expansion, with $3p$ and $3d$ as correlation; the $n=3$ correlation effects are thus excluded from their calculations. Similar to the calculations of O VI, the present bound channel expansion of O VII includes all states corresponding to configurations $3p^2$, $3d^2$, and all two-electron configurations including the orbitals up to $4s$ and $4p$.

The photoionization cross sections for O VIII can be obtained in the hydrogenic approximation using a procedure due to Storey and Hummer [11] and Seaton [12].

The computations are carried out using the *R*-matrix codes developed for the OP [15] and extended for the IP work [19]. The asymptotic code, STGBF, which computes the bound-free transition amplitudes was modified to yield partial, state-specific photoionization cross sections with given initial and final states [13]. The total and the partial cross sections are computed using different algorithms because of differences in usage of computer disk storage. Computations are carried out for all bound states, $S_tL_t\pi_t nl$, where $S_tL_t\pi_t$ is a target state and nl is the outer electron with n, the principal quantum number going from the ground state to 10 (11 for a few symmetries), and $0\leqslant l\leqslant 9$. States lying above the first ionization threshold are usually quasibound autoionizing states, but may be bound states in pure LS coupling; such states are not considered in the present work. Identification of the calculated states is carried out through detailed examination of the effective quantum numbers and channel percentage contributions employing a code ELEVID.

The accuracy of theoretical oscillator strengths for bound-bound transitions may be determined through lifetime values obtained from the computed f values. The lifetimes are often measured with higher precision than the f values. The transition probability, A_{ji}, from state j to i can be obtained from the oscillator strength, f_{ij}, as

$$A_{ji}(\text{a.u.})=\alpha^{3/2}\frac{g_i}{g_j}E_{ij}^2 f_{ij}, \tag{2.2}$$

where E_{ij} is the transition energy in Rydbergs, g_i and g_j are

TABLE III. f values of oxygen ions. Present calculated f values are referred to as P. N_f is the total number of f values for bound-bound transitions below the ionization threshold obtained in this work and under the OP.

Transition	f_{if} Theor.	Expt.
O I: $N_f=1264$ (P), 836 (OP)		
$2p^4(^3P)\rightarrow 2p^3 3s(^3S^o)$	0.0547[P],0.0519 [2],0.0529 [23],0.0537 [24]	0.048 [26],0.048 [29],0.047 [31], 0.048 [35]
$2p^4(^3P)\rightarrow 2p^3 3s(^3P^o)$	0.081[P],0.0794 [2],0.0791 [24]	0.086(0.006) [26]
$2p^4(^3P)\rightarrow 2p^3 3s(^3D^o)$	0.058[P],0.0584 [23],0.0558 [24]	0.061(0.006) [26],0.049 [29],0.054 [31],0.052 [25], 0.062 [35],0.049 [34],0.057 [30]
$2p^4(^3P)\rightarrow 2p^3 4s(^3S^o)$	0.0084[P],0.0091 [2],0.00909 [23],0.0092 [24]	0.01(0.002) [26],0.014 [29],0.0096 [25]
$2p^4(^3P)\rightarrow 2p^3 3d(^3D^o)$	0.023[P],0.0189 [2],0.0212 [23],0.0203 [24]	0.019(0.001) [26],0.029 [29]
$2p^4(^3P)\rightarrow 2s2p^5(^3P^o)$	0.0612[P],0.0624 [2],0.0695 [24]	0.07(0.004) [26]
$2p^4(^1D)\rightarrow 2p^3 3s(^1P^o)$	0.048[P],0.046 [2],0.0484 [24]	0.044(0.026) [25]
$2p^4(^1D)\rightarrow 2p^3 3s(^1D^o)$	0.105[P],0.108 [2],0.109 [24]	0.098 [25],0.112 [35],0.104 [31],0.104 [33],0.099 [34]
O II: $N_f=8603$ (P), 7826 (OP)		
$2s^2 2p^3(^4S^o)\rightarrow 2s2p^4(^4P)$	0.271[P],0.265 [3], 0.270 [47]	
O III: $N_f=8148$ (P), 7740 (OP)		
$2s^2 2p^2(^3P)\rightarrow 2s2p^3(^3D^o)$	0.108[P],0.105 [5]	
$2s^2 2p^2(^3P)\rightarrow 2s2p^3(^3P^o)$	0.143[P],0.135 [5]	
O IV: $N_f=1940$ (P), 1790 (OP)		
$2s^2 2p(^2P^o)\rightarrow 2s2p^2(^2S)$	0.071[P],0.067 [7]	0.052(0.11) [54],0.092(0.028) [52],0.071(0.008) [33], 0.064(0.004) [34],0.080 [28]
O sc v: $N_f=2630$ (P), 2294 (OP)		
$2s^2(^1S)\rightarrow 2s2p(^1P^o)$	0.522[P],0.522 [8]	0.53(0.02) [56]
O VI: $N_f=594$ (P), 306 (OP)		
$2s(^2S)\rightarrow 2p(^2P^o)$	0.198[P],0.198 [9]	0.19(0.04) [54]
O VII: $N_f=1172$ (P), 630 (OP)		
$1s2s(^1S)\rightarrow 1s2p(^1P^o)$	0.6939[P],0.6944 [58],0.695 [10]	

the statistical weights of the initial and final states, and α is the fine-structure constant. Once the A values from an upper state j to all lower states are known, the lifetime of the state j can be obtained as

$$\tau_j=\frac{1}{A_j}, \tag{2.3}$$

where $A_j=\Sigma_i A_{ji}$ is the total radiative transition probability for the state j.

The Rydberg series of autoionizing resonances in the photoionization cross sections are resolved in detail as explained in Ref. [6]. The resonance structures are resolved with $\Delta\nu=0.01$ up to effective quantum number, $\nu=10$. ν, relative to the threshold of convergence, is $\nu(E)=z/\sqrt{(E-E_t)}$ (in Rydberg) where E_t is the target threshold energy and E is the continuum electron energy. The near threshold resonances that contribute predominantly to low-temperature recombination are resolved on a much finer energy mesh with typically 2000 energies just above the ionization threshold. The resonance profiles decrease in width with increase of the effective quantum number as ν^{-3}. The dense, narrow resonances in the energy region between $\nu>10$ and the corresponding target threshold are averaged over using the Gailitis averaging procedure [6].

III. RESULTS AND DISCUSSIONS

The radiative processes in oxygen are studied through all ionization stages. Comparisons and important features for each ion, in particular with those evaluated and compiled recently by the National Institute of Standards and Technology (NIST) [37] are discussed. The computed atomic parameters, the term energies (E), oscillator strengths (f values), and photoionization cross sections, $\sigma_{\rm PI}$, for the oxygen ions, O I–O VII, are expected to be of higher accuracy and provide a more extensive radiative dataset than the previous works. Therefore considerable effort is devoted to ascertain the accuracy of the individual quantities in comparison with experimental data, wherever available, and the best theoretical calculations so far. Each quantity is described in separate subsections below.

TABLE IV. Lifetimes, τ (ns), of oxygen ions. Present results are referred to as P.

State	τ	
	Theory	Expt.
	O I	
$2p^3 3s(^3S^o)$	1.61[P],1.61 [2],1.61 [23]	1.8(2) [33],1.8 [29],1.79(17) [35],1.7(2) [27], 1.70(14) [28]
$2p^3 3s(^3D^o)$	4.11[P],4.39 [2],4.19 [23]	3.94(22) [35],5.0(4) [34],4.5(4) [31]
$2p^3 4s(^3S^o)$	5.74[P],5.26 [2],5.24 [23]	4 [29]
$2p^3 5s(^3S^o)$	13.56[P],12.5 [2],12 [24]	17(3) [40]
$2p^3 6s(^3S^o)$	26.59[P],24.4 [2],25 [24]	24(3) [40]
$2p^3 3p(^3P)$	27.40[P],32.9 [2],29.68 [23],30 [24]	39.1(1.4) [32],36(4) [40],40(3) [36]
$2p^3 3p(^5P)$	26.24[P],29.7 [2],26.99 [23]	39(2) [36]
$2p^3 4p(^5P)$	198.78[P],201 [2],189.7 [23]	193(10) [36],194(19) [39]
$2p^3 4p(^3P)$	161.48[P],175.4 [23],177 [2]	153(10) [36],161(19) [39]
$2p^3 3d(^3D^o)$	8.67[P],9.0 [23],9.89 [2]	9.0 [29]
$2p^3 4d(^3D^o)$	28.77[P],13.5 [2],16.85 [23],15 [24]	23(3) [40],20 [29]
$2p^3 4d(^5D^o)$	72.43[P],73.9 [2],72.2 [23]	96(4) [29],95(9) [39]
$2p^3 5d(^3D^o)$	27.50[P],31.8 [2],$<$15 [24]	36(4) [40]
	O II	
$2p^2 3s(b^4P^e)$	0.987[P],0.956 [3],1.03 [47]	0.9(0.3) [33],0.89(0.05) [34],0.083(0.21) [28]
$2p^2 3s(a^2P^e)$	0.252[P],0.247 [3],0.246 [47]	0.262(0.013) [34],0.27(0.01) [28]
$2p^2(^3P)3p(y^4S^o)$	4.55[P],4.40 [3],4.17 [47]	4.8(0.2) [41],4.8 [43],5.6 [43]
$2p^2 3p(z^4P^o)$	7.24[P],6.97 [3],6.82 [47]	8.8(1.8) [42],6.04(0.34) [46],8.12 [27],8.1 [43]
$2p^2 3p(z^4D^o)$	12.1[P],11.7 [3],10.95 [47]	13.7 [43],15.1(0.8) [44]
$2p^2(^3P)3p(y^2P^o)$	7.49[P],7.36 [3],7.49 [47]	7.3(0.3) [46],6.8(0.1) [45],7.1 [43],9.2(0.1) [44], 6.0(0.5) [41],6.01 [42]
$2p^2(^1D)3p(x^2P^o)$	4.80[P],4.95 [3],4.12 [47]	4.8(0.2) [34],4.96(0.25) [28],4.9 [43]
$2p^2(^3P)3p(y^2D^o)$	10.8[P],10.8 [3],10.8 [47]	9.5(5) [42],11.6(0.3) [44],11.85 [27]
$2p^2(^1D)3p(x^2D^o)$	7.25[P],7.47 [3],6.25 [47]	9.2(0.4) [44],3.7(0.3) [41],3.72 [42]
$2p^2 3p(z^2F^o)$	9.78[P],10.5 [3],8.85 [47]	9.86(0.5) [45],10(1) [41],10.5(1.2) [42]
$2s2p^4(a^4P^e)$	1.15[P],1.19 [3],1.14 [47]	1.2(0.2) [31],1.26(0.1) [35]
$2s2p^4(a^2S^e)$	0.181[P],0.189 [3],0.184 [47]	0.203(0.007) [34],0.21(0.01) [51],0.25(0.03) [33]
$2s2p^4(b^2P^e)$	0.132[P],0.133 [3],0.134 [47]	0.14(0.011) [34],0.16(0.02) [28],0.12(0.03) [33]
$2s2p^4(a^2D^e)$	0.428[P],0.447 [3],0.44 [47]	0.4(0.1) [31],0.45(0.04) [33],0.44(0.08) [35], 0.44(0.04) [34]
$2p^2 3d(c^4P^e)$	0.224[P],0.209 [3],0.236 [47]	0.26(0.02) [50]
$2p^2 3d(a^4D^e)$	4.58[P],4.77 [3],1.55 [47]	4.46 [42],2.9 [43]
$2p^2 3d(a^4F^e)$	4.75[P],5.0 [3] 4.92 [47]	4.9 [43],8.4(0.5) [42]
$2p^2 3d(a^2F^e)$	0.397[P],0.375 [3],0.419 [47]	0.38(0.03) [50],0.37(0.05) [28]
	O III	
$2p3s(y^1P^o)$	0.228[P],0.215 [5],0.226 [48]	0.17(0.01) [49],0.227(0.011) [50]
$2p3s(y^3P^o)$	0.262[P],0.253 [5]	0.266(0.011) [50]
$2p4s(w^1P^o)$	0.351[P],0.320 [5]	0.350 [34]
$2s2p^3(z^1P^o)$	0.080[P],0.090 [5]	0.087(0.006) [34]
$2s2p^3(z^1D^o)$	0.175[P],0.183 [5]	0.2(0.05) [34],0.2 [54]
$2s2p^3(z^3S^o)$	0.064[P],0.069 [5]	0.079(0.04) [34]
$2s2p^3(z^3P^o)$	0.484[P],0.530 [5]	0.575(0.018) [34]
$2s2p^3(z^3D^o)$	1.57[P],1.63 [5]	1.61(0.07) [34]
$2p3p(a^3S^e)$	2.19[P],2.15 [5]	2.85(0.46) [45]
$2p3p(c^3P^e)$	3.83[P],2.77 [5]	3.03(0.18) [52]
$2p3p(a^3D^e)$	5.11[P],4.94 [5]	4.62(0.24) [52]
$2s2p^2 3s(a^5P^e)$	0.306[P],0.302 [5]	0.32(0.03) [50]

TABLE IV. (*Continued.*)

State	τ	
	Theory	Expt.
	O IV	
$2s^2 3s(b^2S^e)$	0.131[*P*],0.125 [7]	0.137(0.01) [50]
$2s2p3s(x^2P^o)$	1.40[*P*],0.144 [7]	1.41(0.05) [50]
$2s2p3s(z^4P^o)$	0.0983[*P*],0.0966 [7]	0.101(0.005) [50]
$2s2p^2(a^2S^e)$	0.249[*P*],0.266 [7]	0.36(0.08) [53],0.29(0.2) [34]
$2s2p4f(a^4G^e)$	0.245[*P*],0.244 [7]	0.24(0.03) [30]
	O V	
$2s2p(^1P^o)$	0.333[*P*],0.333 [8]	0.336(0.015) [56],0.38(0.02) [34]
$2p^2(^1S)$	0.242[*P*],0.237 [8]	0.29(0.03) [33],0.28(0.02) [34],0.285(0.03) [57]
$2p^2(^3P)$	0.436[*P*],0.434 [8]	0.45(0.03) [34]
$2p^2(^1D)$	3.05[*P*],3.05 [8]	3.2(0.2) [33],2.7(0.2) [34]
$6h(z^1H^o)$	0.971[*P*]	1.0(0.1) [55]
	O VI	
$2p(z^2P^o)$	2.45[*P*],2.45 [34]	2.5 [54]
$7f(w^2F^o)$	0.291[*P*]	0.31(0.02) [55]
	O VII	
$1s3s(b^3S)$	44.3[*P*]	65(6) [59]
$1s3p(y^3P^o)$	18.75[*P*]	19.2(2) [59],21 [60]
$1s4p(x^3P^o)$	31.64[*P*]	31.2(2) [59]
$1s3d(a^1D)$	6.57[*P*]	8(1.5) [59],12 [60]
$1s4d(b^1D)$	15.51[*P*]	16.2(1.5) [59]
$1s5d(c^1D)$	29.97[*P*]	28(2) [59]
$1s3d(a^3D)$	6.20[*P*]	7(1) [59],15 [60]
$1s4d(b^3D)$	14.29[*P*]	16(1.5) [59],21 [60]
$1s5d(c^3D)$	27.49[*P*]	31(3) [59]
$1s6d(d^3D)$	46.76[*P*]	47(3) [59]

A. Energies

Comparison of the first 20 lowest bound states of each ion is made in Table II. The total number of calculated bound states, N_b, below the ionization threshold with $n \leqslant 10$ and $\ell \leqslant (n-1)$ is quoted for each ion in the table. The OP numbers are also given for comparison. Present calculated energies for O I are of comparable accuracy with those by Butler and Zeippen [2] in agreement with the observed ones [21]. Present work obtains 107 bound states of O I below the ionization threshold, compared to 69 obtained in their work. The 12-CC eigenfunction expansion has resulted in 296 possible bound states of O II below the ionization threshold, which is 77 more than the 219 obtained in the most detailed previous study by Burke and Lennon [3]. Comparison of the energies in Table II shows good agreement, slightly better for most cases than those by the previous calculated values [3], with the measured values [22]. The 23-CC eigenfunction expansion, including states from the $n=3$ complex, is considerably larger than the 8-CC expansion used by Luo *et al.* [5] in the most intensive study prior to this work. The computed energies for the 296 bound states of O III below the ionization threshold (compared to 267 in the earlier work) agree well with the experimentally measured values [21]. The calculations for O IV using a 12-CC eigenfunction expansion have resulted in a total of 109 bound states. The energies are compared with the 6-CC calculations by Fernley *et al.* [7]. Present energies agree very well with those of Fernley *et al.* and of the measured ones [21]. However, a few excited states with excited core state $2s2p(^1P^o)$, e.g., $2s2p(^1P^o)3s(^2P^o)$, show larger difference, 7% for the specified state, compared to those by Fernley *et al.* The present energies for O V are in very good agreement with the measured values [21] as well as with those by Tully *et al.* [8]. The earlier 2-CC calculations for O VI by Peach *et al.* [9] is limited to states with highest angular momentum of $L=2$. Present 11-CC calculations obtain 51 bound states, which are in very good agreement with the measured values [21]. The calculated energies of O VII obtained using 10-CC calculations are also in very good agreement with the measured values [21].

B. Oscillator strengths and lifetimes

The oscillator strengths (f values) and photoionization cross sections are obtained in a consistent manner to reduce the uncertainties in various applications, such as in total photoabsorption and electron-ion recombination processes, where both quantities are needed. It is also important to cal-

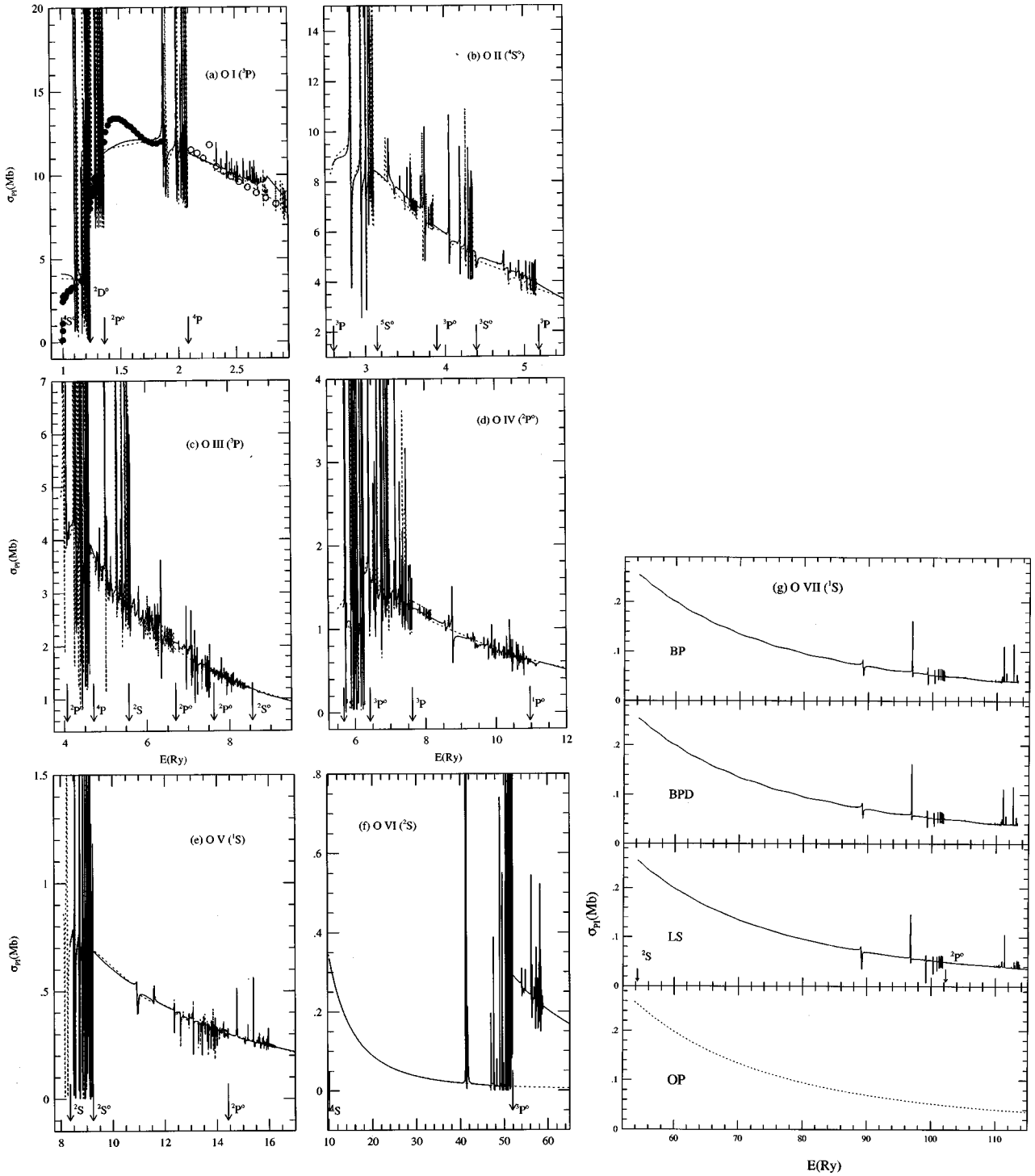

FIG. 1. Total photoionization cross sections σ_{PI} of the ground state of oxygen ions, solid curves: present work; dotted curves: OP: (a) O I (OP Ref. [2]), the filled (new) and open (earlier) circles are the measured values of Angel and Samson [38]; (b) O II (OP Ref. [3]); (c) O III (OP Ref. [5]); (d) O IV (OP Ref. [7]); (e) O V (OP Ref. [8]); (f) O VI (OP Ref. [9]); (g) O VII (OP Ref. [10]). Arrows point to various target states.

culate a more complete set of radiative transition probabilities as required by collisional-radiative models for accurate analysis of spectra from astrophysical and laboratory plasmas. The number of transitions obtained for each ion in the present work is much larger than the existing data for these ions. The *f* values for the oxygen ions are compared with the available experimental and accurate calculated values in Table III. Although a large number of *f* values are obtained, including those for transitions among bound and quasibound states, only those transitions among pure bound-bound states are discussed and presented. Total number of transitions, N_f, below the ionization threshold for each ion is specified in Table III. Comparison of lifetimes obtained from the *f* values is given in Table IV. There are more measured values of lifetime available than the *f* values.

Present *f* values for O I are in good agreement with those of Butler and Zeippen [2] and of atomic structure calculations of Hibbert *et al.* [23] for most of the transitions, such as

for transitions $2p^4(^3P) \rightarrow 2p^3 3s(^3D^o)$ and $2p^4(^1D) \rightarrow 2p^3 3s(^1D^o)$ (Table III). The f values are within the range of the measured values except for the resonant (i.e., the lowest dipole) transition, $2p^4(^3P) \rightarrow 2p^3 3s(^3S^o)$, for which the present value is about 14% higher and Ref. [2], which is rated to be accurate to within 3% by the NIST compilation [37], is 9% higher than the measured value. The calculated lifetimes derived from the f values are in good agreement with the calculated values of Refs. [2] and [23] and within or close to the measured values for most of the states. Although the calculated values are consistent with each other for states such as $2p^3 4s(^3S^o)$, $2p^3 3p(^5P^o)$, and $2p^3 4d(^5D^o)$, they differ from the measured values, e.g., the present lifetime for $2p^3 4s(^3S^o)$ differs from the other calculated values by 4% but is higher than the measured value by 37%. The number of oscillator strengths obtained for bound-bound transitions below the ionization threshold for O I is 1264, which is about 50% more than 836 obtained by Butler and Zeippen [2].

Comparison of O II f values shows that the present f value, 0.271, for the resonant transition $2s^2 2p^3(^4S^o) \rightarrow 2s2p^4(^4P)$ agrees quite well with the value 0.270 obtained by Bell *et al.* [47], that has been rated to be accurate to within 10% by NIST [37]; the Ref. [3] value is also close, 0.265. The computed lifetimes are within the measured values of various experiments, with a few exceptions (Table IV). Among the states with large discrepancies is the $2p^2 3p(z^4D^o)$ for which the present lifetime is 12.1 ns and is lower than the measured values of 13.7 ns [43] and 15.1(0.8) ns [44], but still is in slightly better agreement with the measured values than the calculated values of 11.7 ns by Burke and Lennon [3], and 10.95 ns by Bell *et al.* [47]. Number of oscillator strengths in this work, 8603, is also larger than 7826 obtained in Ref. [3].

The f values for the transitions $2s^2 2p^2(^3P) \rightarrow 2s2p^3(^3P^o, ^3D^o)$ of O III agree very well with Luo and Pradhan [5] values, rated accurate within 3% by NIST [37]. The lifetime values agree within the uncertainty of the experimental values for most of the states in Table IV. The largest discrepancy is seen to be with state $2p3p(c^3P^e)$, for which the present lifetime is 3.83 ns compared to the measured value of 3.03(0.18) ns [52] and 2.77 ns obtianed by Luo and Pradhan. The lifetime for the $2p3s(^1P^o)$ state of O III has been measured using a beam-foil technique by Pinnington *et al.* [51] and more recently by Baudinet-Robinet *et al.* [49]. The calculated lifetime for this state agrees with Pinnington *et al.* and other theories, such as with Luo and Pradhan [5] and Aggrawal and Hibbert [48], but is higher than the recent measured value by about 23%.

The f value and lifetimes for O IV are well within or close to the available calculated and measured values. The present f value for the transition $2p(^2P^o) \rightarrow 2s2p^2(^2S)$ (Table III) and the lifetimes of states $2s^2 3s(^2S)$, $2s2p3s(^2P^o, ^4P^o)$, $2s2p4f(^4G)$ (Table IV) are all within the measured values of the various experiments except the lifetime of $2s2p^2(^2S)$, which is lower than the measured values by 7–11 %.

The f value for the resonant transition of O V, $2s^2(^1S) \rightarrow 2s2p(^1P^o)$, agrees very well with other calculated values and the measured value. The lifetimes are also show very good agreement between the calculated and measured values (Table IV), except for the lifetime of $2p^2(^1S)$ for which both calculations yield 0.24 ns, which is 8% lower than the lowest of the measured values, 0.26 ns.

The number of present f values obtained for transitions among the bound states below the ionization threshold of O VI is 594 compared to 306 obtained by Peach *et al.* [9]. The f value for the resonant transition $1s^2 2s(^2S) \rightarrow 1s^2 2p(^2P^o)$ agrees very well with other calculated values. The lifetimes of $2p(^2P^o)$ and $7f(^2F^o)$ states are also within the experimentally measured values.

The present f value, 0.694, for the resonant transition of O VII, $1s^2(^1S) \rightarrow 1s2p(^1P^o)$, agrees very well with the variationally determined relativistic calculations of Cann and Thakkar [58], 0.6944, rated accurate within 1% by NIST compilation [37], as well as with that of Fernley *et al.* [10]. The lifetimes are compared with the latest beam-foil measurements of Trabert *et al.* [59] and Buchet *et al.* [60] who also used a beam-foil technique. Present lifetimes agree very well with the latest values of Trabert *et al.* except for the state $1s3s(^3S)$ where the lower limit of the measured value is 25% higher than the calculated value.

C. Photoionization

As a function of photon energy, both the forms of $\sigma_{\rm PI}$ are obtained: the *total* cross section for leaving the residual core ion in all accessible target states in the CC expansion, and the *partial* cross section leaving the core ion in the ground state alone. *Total* cross sections are needed in applications, such as in plasma ionization balance equations in photoionization equilibrium, and the *partial* cross sections are needed in applications, such as in the calculations of recombination cross sections where an incident electron combines with an ion in its ground state. The number of bound states for which total $\sigma_{\rm PI}$ are obtained is the same as the number of possible bound states, N_b. However, the number of *partial* photoionization cross sections is usually less than that of the *total* photoionization cross sections since not all the bound states of an ion may couple to the ground state of the residual ion.

1. Ground-state photoionization

Ground-state photoionization cross sections usually have less resonance features compared to those of excited states. Present photoionization cross sections, $\sigma_{\rm PI}$, for the ground state of each ion do not differ considerably in the background, except for O VI, from the earlier calculations although different eigenfunction expansions have been used. The cross sections are shown in Figs. 1(a)–1(g) where the solid curves are the present values and the dotted ones are from earlier works. ($\sigma_{\rm PI}$ of H-like O VIII can be obtained from TOPbase.) In Fig. 1, the ionization threshold as well as various target thresholds are pointed out by arrows. They display the relevant features such as the convergence of Rydberg series of resonances on to the individual excited states of the target ion; for example convergence at the $2s2p^4(^4P)$ threshold of O II in the photoionization of O I [Fig. 1(a)] and at $2s2p^3(^5S^o)$ threshold of O III for $\sigma_{\rm PI}$ of O II [Fig. 1(b)].

Some significant features of the cross sections are seen. $\sigma_{\rm PI}$ of O I exhibits a considerable rise at the threshold $2p^3(^2P^o)$ of O II [Fig. 1(a)]. Similar enhancement is seen at the $2s2p(^3P^o)$ threshold for O IV [Fig. 1(d)]. The large enhancement for O VI cross sections at the $1s2p(^2P^o)$ thresh-

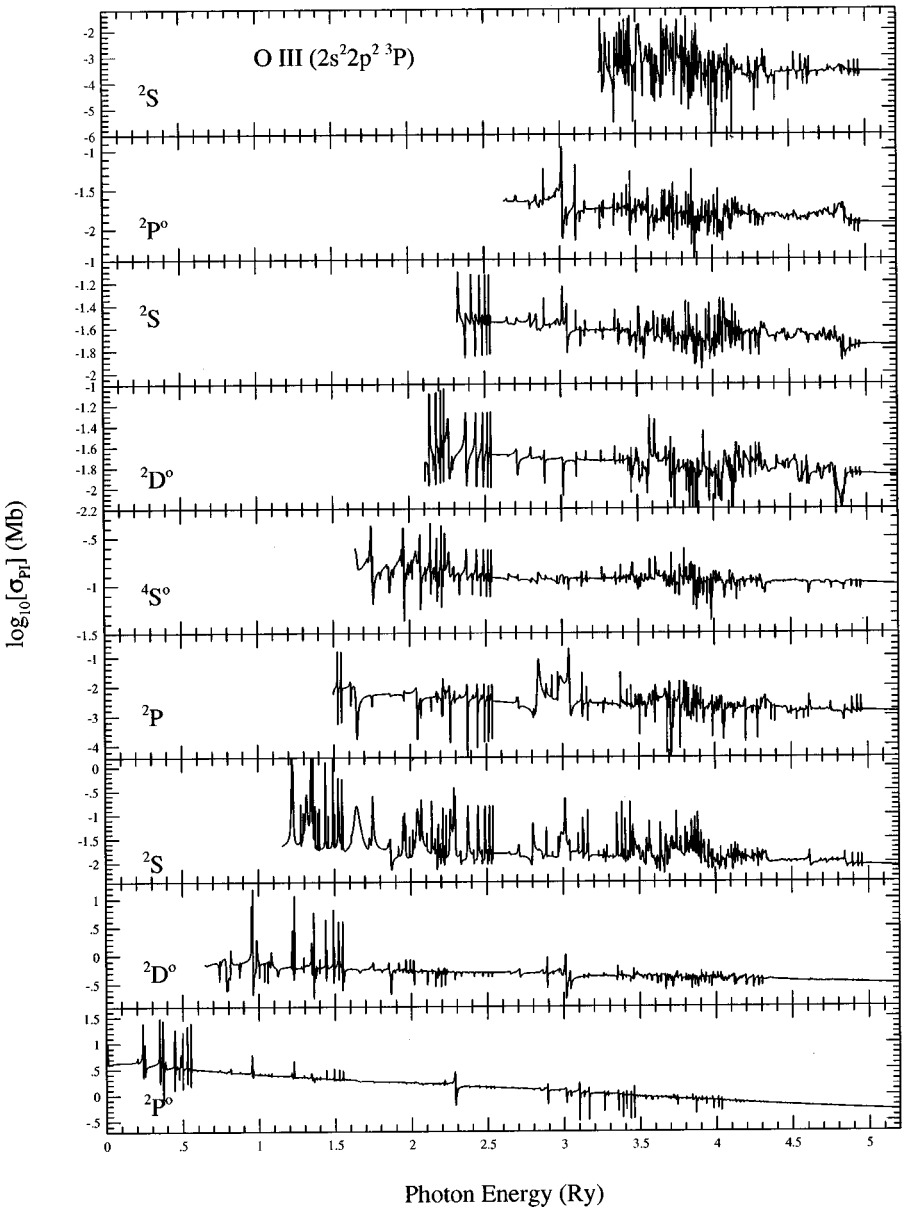

FIG. 2. Partial photoionization cross sections of the ground state of O III leaving the residual ion in the states specified in each panel.

old, differing considerably from the earlier work [Fig. 1(f)] is due to the opening of the 1*s* shell of the core ion O VII.

There have been several experimental measurements of the ground-state photoionization cross section of O I, most recently by Angel and Samson [38] using a synchrotron radiation source. However, recent experiments show a persistent disagreement with the best theoretical calculations to date (e.g., [2,18]) using the CC approximation. Comparison of theoretical and measured values is presented in Fig. 1(a) where the solid curve represents the present cross sections, the dotted one those of Butler and Zeippen [2]. The cross sections of Bell *et al.* also agrees closely with the present calculated values. The filled circles are the new measured values and the open circles are the previous measured values fitted to new data by Angel and Sampon [38]. The discrepancies are twofold: (i) in the near-threshold region the experimental values are approximately 37% lower, and (ii) a ''hump'' feature above the $2p^3(^2P^o)$ threshold observed in the experimental results but not in the theoretical calculations. Further investigation is required.

Comparison with the earlier calculations shows generally good agreement for most of the oxygen ions. However, significant differences are found in the resonance structures in the near threshold regions for O III, O IV, and O V, which will affect photoionization and recombination rates at very low temperatures. Present cross sections also show more narrow resonances on otherwise smooth backgrounds in the high-energy region because of the added terms in the target expansions. The large difference in O VI, Fig. 1(f), is due to negligence of the excited correlation terms by Peach *et al.* [9], thereby underestimating the cross sections by a considerable amount in the high-energy region.

Photoionization cross sections for O VII should be of particular interest in x-ray spectroscopy of laboratory and astrophysical sources since the He-like ionization stages emit copiously in the x ray; the ionization balance calculations in radiatively ionized sources require accurate photoionization cross sections at high energies. The earlier work for O VII by Fernley *et al.* [10] employs essentially a one-state calculation (their 2-CC calculation consisted of one excited pseu-

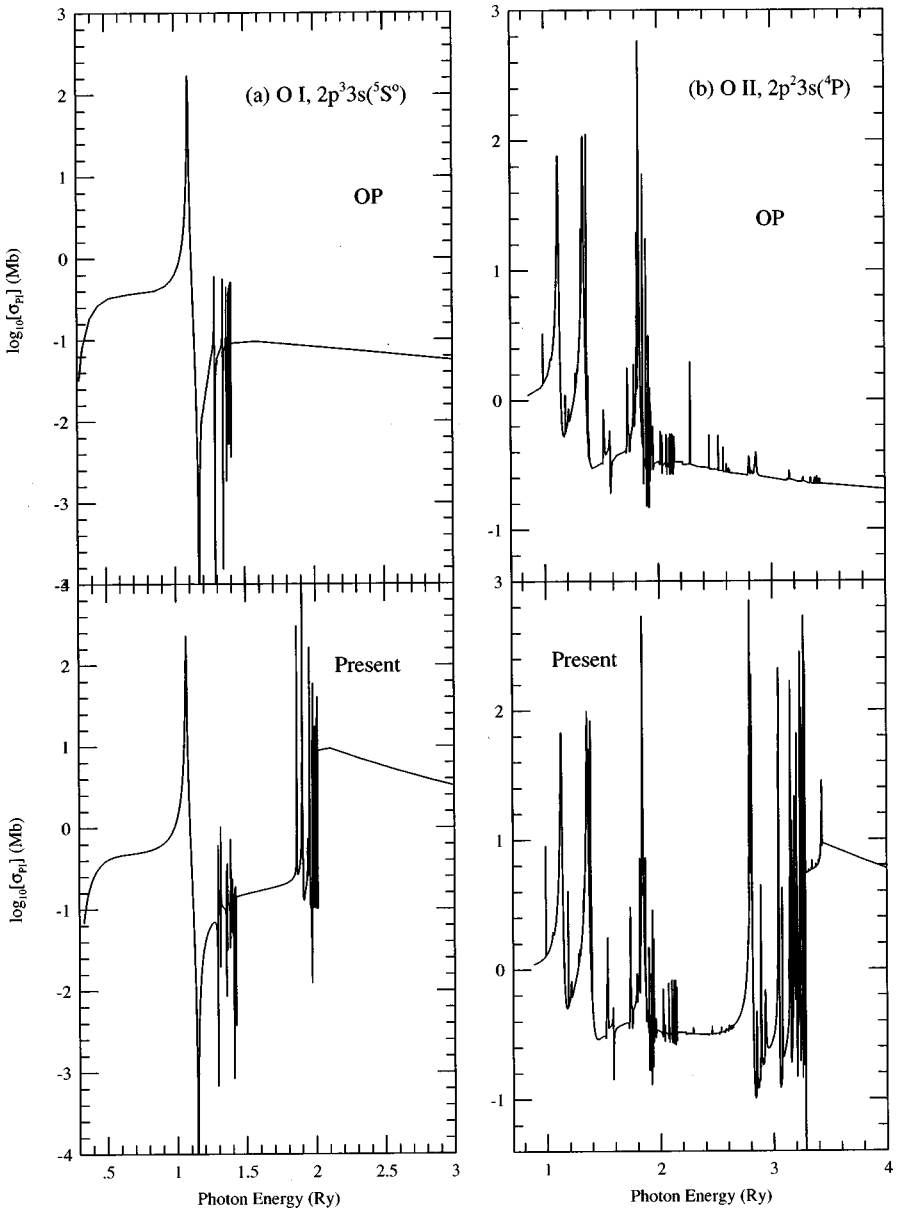

FIG. 3. Comparison of the present photoionization cross sections σ_{PI} of excited states (in the bottom panel of each subplot) for the oxygen ions with those of the OP (upper panels): (a) $2p^3 3s(^5S^o)$ state of O I (OP Ref. [2]), (b) $2p^2 3s(^4P)$ state of O II (OP Ref. [3]), (c) $2p3s(^1P^o)$ state of O III (OP Ref. [5]), (d) $2s2p3s(^4P^o)$ state of O IV (OP Ref. [7]), (e) $2s6d(^1D)$ state of O V (OP Ref. [8]), (f) $1s^2 2p(^2P^o)$ state of O VI (OP Ref. [9]), (g) $1s2s(^1S)$ of O VII (OP Ref. [10]).

dostate), and therefore no resonance structures is included [lowest panel of Fig. 1(g)]. We discuss photoionization of O VII in some more detail in the following subsection.

2. Relativistic and radiation damping effects

For a highly charged ion, two factors may become important for computation of σ_{PI}: (i) the relativistic and (ii) the radiation damping effects, in which case LS coupling may not be a good approximation. Relativistic effects will introduce more resonances because of fine structure splitting of core LS states. Radiation damping of the quasibound states will reduce the autoionization probability lowering the peaks of the resonances. We investigate both of these effects on O VII in Ref. [61] using the Breit-Pauli approximation for relativistic effects [62] and radiative damping of resonances in photoionization cross sections [63]. O VII is a highly charged ion with a H-like residual core that has comparatively high radiative decay rates ($\sim 10^{12}$ sec^{-1}) for dipole transitions between the lowest core levels. Although the radiative decay rate is still lower than the typical autoionization rate of $\sim 10^{14}$ sec^{-1}, the autoionizing resonances are expected to undergo some radiative damping and their effect in enhancing the photoionization cross section would be reduced.

Figure 1(g) has four panels that present ground-state photoionization cross sections of O VII obtained (i) in the relativistic Breit-Pauli (BP) approximation using a 16-CC expansion (BP, top panel), (ii) in BP approximation, but including radiation damping effects (BPD, second panel), and (iii) in LS coupling (LS, third panel) all of which look very similar. (σ_{PI} in the fourth panel under the OP is stated in the above section.) The resonance peaks in BP and BPD have about the same heights, indicating negligible radiation damping. Although very similar in features, small differences can be noticed in σ_{PI} between BPD (or BP) and LS, such as the last peak which is high in BP and BPD, but is much lower in LS. Resonances that are even narrower than the ones shown (i.e., with smaller autoionization width), may undergo radiation damping but that effect on the photoionization cross sections would be negligible. The overall effect of these

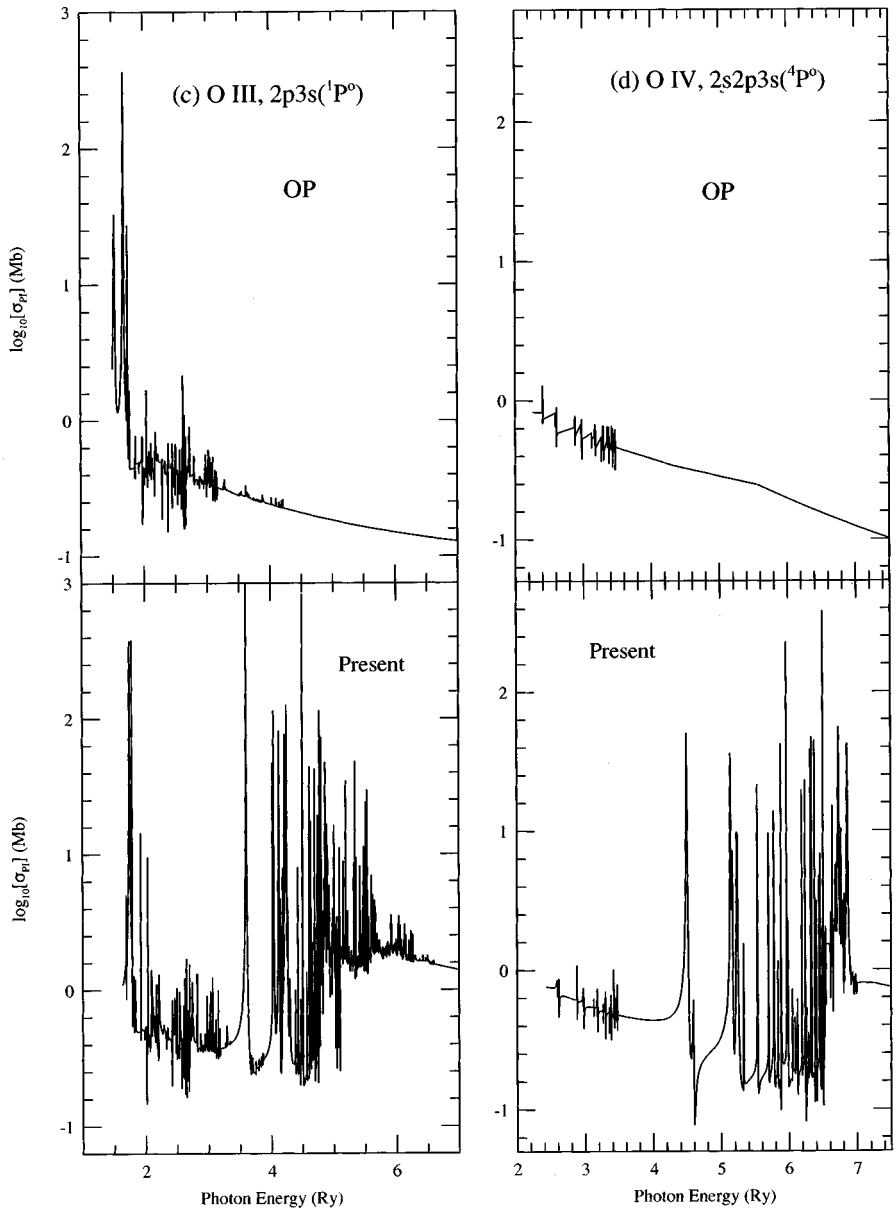

FIG. 3. (*Continued*).

small differences is further investigated in applications such as on total electron-ion recombination cross sections [61] and rates [65]. The BP rates without the radiation damping effect are larger than those in LS coupling. However, inclusion of the damping of resonances reduces these rates back to roughly those in LS coupling; the maximum difference between the two sets is only about 6% [65]. The fine structure and resonance damping operate in an opposite manner and their combined effect does not make any significant contributions to the photoionization cross sections of oxygen ions.

3. Partial cross sections

The partial cross sections for photoionization of the ground state into the ground and various excited states of the residual core ion are needed in the determination of level populations in non-local-thermodynamic-equilibrium (non-LTE) atomic models of plasma sources. The dominant ionization is usually into the ground state of the core, with cross sections almost equal to that of the total over a wide energy range. An illustrative example is shown in Fig. 2 for O III. O III is one of the most important ions in gaseous nebulae and other astrophysical objects [64]. Each panel in Fig. 2 corresponds to photoionization with the resultant core state specified in the panel. Although the background partial cross sections with excited cores are much weaker than those with the ground core, extensive resonance structures in these cross sections correspond to strong autoionization into these excited levels.

4. z dependence

Hydrogenic atomic systems exhibit z- (ion charge) dependent behavior; their energies vary as z^2/n^2, the transition probabilities for bound-bound and bound-free transitions vary as z^2/n^3. Hence, it of interest to find whether any such trend exists in a sequence with increasing ion charge so that predictions can be made for the higher charged members. In

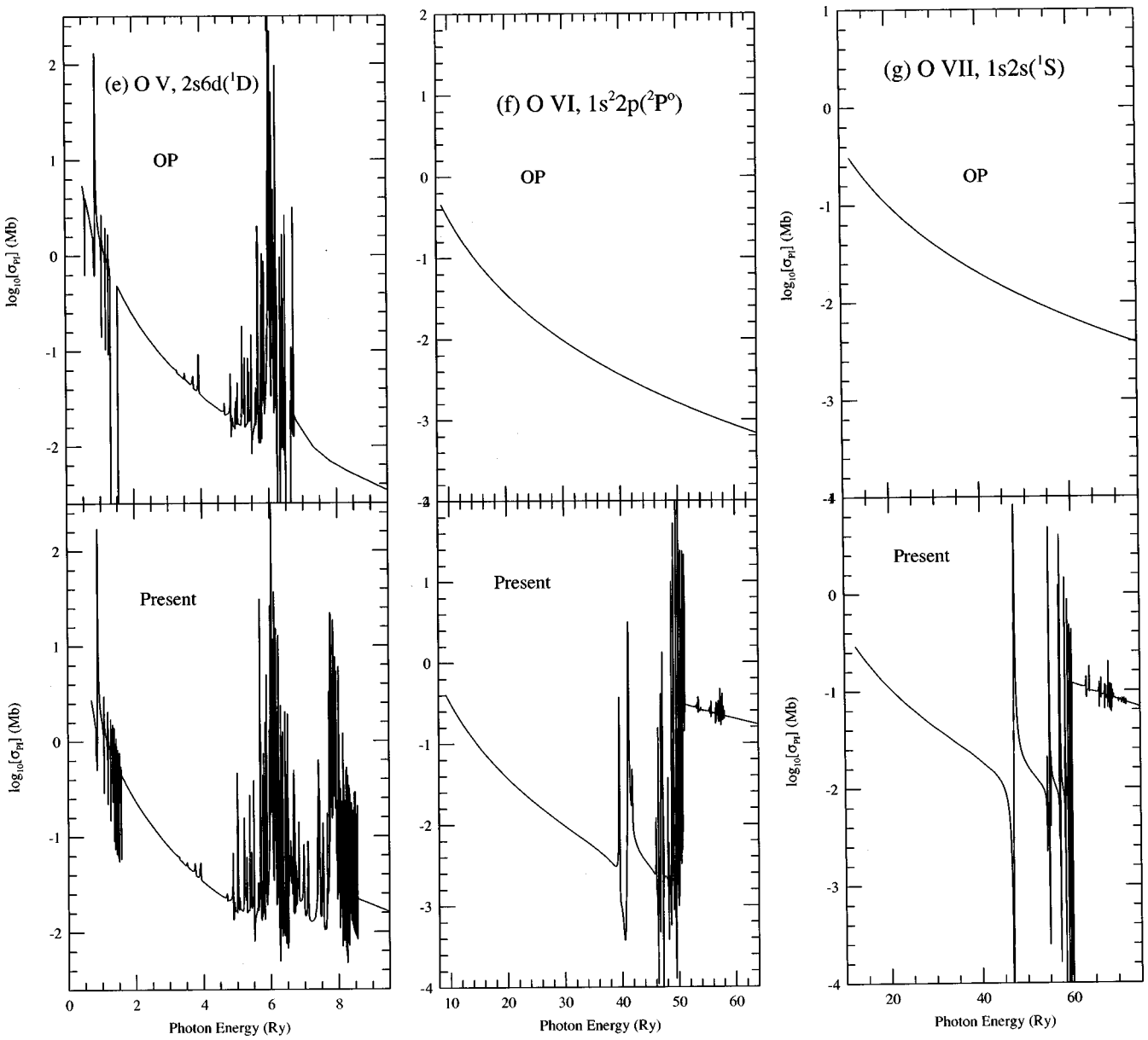

FIG. 3. (*Continued*).

contrast to hydrogenic systems multielectron systems are affected by the complex electron-electron correlations that modify the attractive nuclear Coulomb force of the ion. Also the quasibound states of the Rydberg series belonging to excited core thresholds of multielectron systems introduce resonance structures in the collision processes. However, an isoelectronic sequence of ions, for which the number of electrons remains the same, shows some z-dependent behavior for some cases such as in ground-state photoionization cross sections [6]. The behavior is usually more prominent when the ion charge is higher, i.e., when the nuclear Coulomb force is comparatively stronger. In a previous study of background cross sections of ground-state photoionization of highly charged carbon isoelectronic sequence, we found z^2-dependent behavior for the more highly charged members [6]. In order to discern any such behavior for an isonuclear sequence, similar studies with z- and z^2-scaled cross sections are carried out for the present case. However, with the exception of the background cross sections decreasing systematically with increasing ion charge, no z-dependent behavior is revealed for the oxygen isonuclear sequence. This shows that the electron correlation effects associated with the specific configuration in each ion determines the photoionization rather than the effective nuclear charge as in an isoelectronic sequence.

D. Excited-state photoionization

Excited-state photoionization cross sections obtained in the present work for the oxygen ions exhibit more extensive resonances, and often more enhanced background, in the high-energy region than the earlier works, e.g., in the OP calculations. Examples illustrating new features in comparison with the earlier calculations are presented in Figs. 3(a)–3(g) where the top panels present the work under the OP and lower ones the present work.

Figure 3(a) shows the comparison of photoionization cross sections of the excited metastable state, $2p^3 3s(^5S^o)$ of

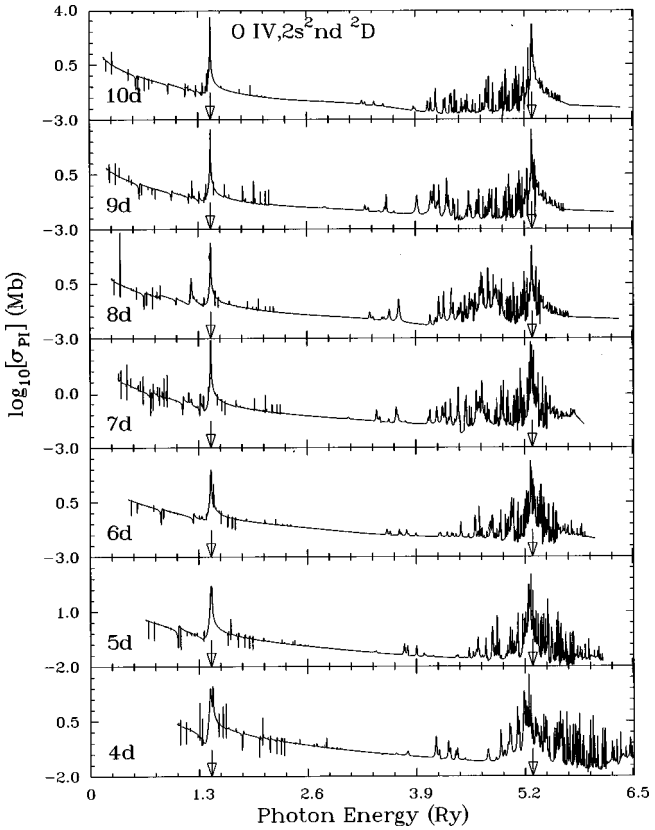

FIG. 4. Photoionization cross sections $\sigma_{\rm PI}$ of the Rydberg series of bound states of O IV, $2s^2nd(^2D)$, with $4d \leqslant nd \leqslant 10d$. The PEC resonances, indicated by the arrows in each panel, are due to the dipole core transitions $2p^3(^4S^o) \rightarrow 2s2p^4(^4P)$ and $2p^23s(^4P)$ in O V (with the exception of the top panel the upper limit is not shown on the y axis).

O I. Computations of $\sigma_{\rm PI}$ for O I include terms in the expansions that were excluded in the earlier work by [2] but included by Bell *et al.* [18]. However, Bell *et al.* confined their study only to the three states of the ground configuration $2s^22p^4$. Correlation of the $n=3$ states provide important contributions by enhancing the background cross sections, as well as introducing more resonances.

The photoionization cross sections of excited O II states, especially the ones above the lowest state of a given symmetry, $SL\pi$, show a considerable difference from the calculations of Burke and Lennon [3] in the high-energy region. The difference is mainly due to inclusion $n=3$ states in the target expansion. Figure 3(b) shows the photoionization cross sections of the excited $2s^22p^23s(^4P^e)$ state of O II. The structures in both the panels look very similar until the target threshold $2s2p^3(^1P^o)$ above which the resonances due to $3s$ states, $2p3s(^3P^o,^1P^o)$, enhance the background cross sections by more than an order of magnitude compared to that of Ref. [3] in the high-energy region.

Inclusion of more states in the wave-function expansion of O III shows pronounced effects in the photoionization cross sections of excited states. Figure 3(c) presents $\sigma_{\rm PI}$ for the excited $2p3s(^1P^o)$ state of O III, which is compared with that of Luo and Pradhan [5]. The increment in the number of target states increases the resonances in $\sigma_{\rm PI}$ due to the doubly excited autoionizing Rydberg series of states belonging to the target thresholds.

Photoionization cross sections of O IV also include more resonances from the Rydberg series belonging to higher target states than in Ref. [7]. An example is $\sigma_{\rm PI}$ of the excited $2s2p3s(^4P^o)$ state shown and compared in Fig. 3(d). The additional resonances in the present $\sigma_{\rm PI}$ raise the effective background cross sections by up to a factor of 7 in the high-energy region.

Photoionization cross sections of a comparatively highly excited state, $2s6d(^1D)$ of O V, are compared with those of Tully *et al.* in Fig. 3(e) to illustrate the effects of target states of a higher complex in the high-energy region. $\sigma_{\rm PI}$ in both panels are similar in feature, except for the difference in the resolution of resonances, up to an energy 6.15 Ry of target state $1s^23d(^2D)$. However, beyond this energy, while the earlier cross sections decrease smoothly in the high-energy region, the present cross sections show extensive resonances due to Rydberg series of autoionizing states belonging to the target thresholds of the $n=4$ complex, and enhanced background cross section by over a factor of 4. It may also be noted that there are two narrow gaps of missing cross sections in the OP cross section, right below the target thresholds of $2p(^2P^o)$ ($\sim$1.5 Ry photon energy) and of $3p(^2P^o)$ ($\sim$ 6.6 Ry of photon energy). Such gaps exist in their cross sections for some other excited states of O V; these gaps were introduced by computational errors during Gailitis averaging of resonances below these thresholds. Hence the present cross sections of O V are more complete and accurate than those of Tully *et al.*, which are currently the best ones available as part of the OP data in TOPbase [4].

Photoionization cross sections, $\sigma_{\rm PI}$, of the excited $1s^22p(^1P^o)$ state of O VI is shown in Fig. 3(f) and compared with those by Peach *et al.* [9]. $\sigma_{\rm PI}$ decreases monotonically in the low-energy region before the Rydberg series of resonances begin to appear. The resonances enhance the background cross section considerably as the inner-shell ionization turns on. However, the earlier cross section by Peach *et al.* [9] continues to decay with energies and miss out all the resonances and the enhancement. As mentioned before, their 2-CC calculation is in fact a one-state calculation and does not include any correlation effects, and thereby underestimates $\sigma_{\rm PI}$ considerably at higher energies.

Photoionization cross section of a hydrogenic ion, such as O VII, has a long smooth curve without any resonances that decrease monotonically with energy since the excited target states are quite high from the ground state. However, as the photon energy approaches near the excited core states, high but narrow resonances of Rydberg series of autoionizing states appear and the effective cross section can be enhanced considerably in the high-energy region. These are seen in $\sigma_{\rm PI}$ for the low-lying state, $1s2s(^1S)$, of O VII [bottom panel of Fig. 3(g)]. There are no resonance structures or enhancement in the results by Fernley *et al.* [10] [top panel of Fig. 3(g)] since (as for O VI) no higher target states were included.

Finally, an example of the effect of PEC resonances in the photoionization cross sections of excited states is shown in Fig. 4. PECs are large structures in photoionization cross sections at high energies. Their contributions to various applications may be significant in the high-energy region. Figure 4 presents $\sigma_{\rm PI}$ of the series of excited states, $2s^2nd(^2D)$ where $4d \leqslant nd \leqslant 10d$, of O VI. The arrows point to the energies of the PEC resonances corresponding to the dipole al-

lowed transitions of the target ground state, $2s^2(^1S)$, to states $2s2p(^1P^o)$ and $2s3p(^1P^o)$. The attenuation of the background cross sections by orders of magnitude is evident. It may be noted that the entire complex of resonances due to the target $n=3$ states, beyond 2.62 Ry in photoelectron energy, is missing from the OP data.

IV. CONCLUSION

A comprehensive study of radiative processes in the oxygen isonuclear sequence, O I–O VII, is carried out using the *R*-matrix method. Consistent and extensive sets of atomic parameters E, f values, and $\sigma_{\rm PI}$ are obtained. Present CC eigenfunction expansions are more complete than those used in the previous calculations. A much larger amount of radiative data are obtained than that of the existing OP data (such as present in the database TOPbase [4]), and should provide more complete datasets for the analysis of astrophysical and laboratory spectra. The level of accuracy of the energy values and the oscillator strengths are better than or comparable to those of the existing values. However, wave function expansions employed yield photoionization cross sections with important features that are missing from earlier results. In particular, the high-energy region $\sigma_{\rm PI}$ reveals that the earlier cross sections have been underestimated for many excited bound states and important PEC features are missing. It may now be possible to investigate cross sections experimentally with advanced technology. Present results have been implemented in the calculations of total recombination rate coefficients and ionization fractions in plasmas in coronal equilibrium [65].

TOPbase may be accessed via telnet as follows: (i) In USA, IP: 128.183.101.54 or topbase.gsfc.nasa.gov, login: topbase, pw: Seaton+; (ii) in Europe (at CDS), IP: 130.79.128.5, login: topbase, pw: Seaton+.

ACKNOWLEDGMENTS

I would like to thank Professor Anil K. Pradhan for discussions, A. F. Robey, and Dr. J. R. Fuhr from NIST for providing their most recent compilation of observed energy values electronically. This work was partially supported by the NSF (AST-9870089) and NASA (NAGS-6908). Part of the computational work was carried out on the Cray YMP at the Ohio Supercomputer Center.

[1] M.J. Seaton, J. Phys. B **20**, 6363 (1987).
[2] K. Butler and C.J. Zeippen (to be published); data available at TOPbase, Ref. [4].
[3] V.M. Burke and D.J. Lennon (to be published); the data are available through the OP database TOPbase, reference is given below.
[4] W. Cunto, C. Mendoza, F. Ochsenbein, and C.J. Zeippen, Astron. Astrophys. **275**, L5 (1993) (TOPbase).
[5] D. Luo, A.K. Pradhan, H.E. Saraph, P.J. Storey, and Y. Yu, J. Phys. B **22**, 389 (1989); D. Luo and A.K. Pradhan, *ibid.* **22**, 3377 (1989).
[6] S.N. Nahar and A.K. Pradhan, Phys. Rev. A **44**, 2935 (1991); **45**, 7887 (1992).
[7] J.A. Fernley, A. Hibbert, A.E. Kingston, and M.J. Seaton (to be published); the data are available through TOPbase [4].
[8] J.A. Tully, M.J. Seaton, and K.A. Berrington, J. Phys. B **23**, 3811 (1990).
[9] G. Peach, H.E. Saraph, and M.J. Seaton, J. Phys. B **21**, 3669 (1988).
[10] J.A. Fernley, K.T. Taylor, and M.J. Seaton, J. Phys. B **20**, 6457 (1987).
[11] P.J. Storey and D.G. Hummer, Comput. Phys. Commun. **66**, 129 (1992).
[12] M.J. Seaton (to be published); the data are available through TOPbase [3]).
[13] S.N. Nahar and A.K. Pradhan, Phys. Rev. A **49**, 1816 (1994); S.N. Nahar and A.K. Pradhan, Astrophys. J. **447**, 966 (1995).
[14] S.N. Nahar and A.K. Pradhan, Astrophys. J., Suppl. Ser. **111**, 339 (1997).
[15] K.A. Berrington, P.G. Burke, K. Butler, M.J. Seaton, P.J. Storey, K.T. Taylor, and Yu. Yan, J. Phys. B **20**, 6379 (1987).
[16] Yu Yan and M.J. Seaton, J. Phys. B **20**, 6409 (1987).
[17] W. Eissner, M. Jones, and N. Nussbaumer, Comput. Phys. Commun. **8**, 270 (1974).
[18] K.L. Bell, P.G. Burke, A. Hibbert, and A.E. Kingston, J. Phys. B **22**, 3197 (1989).
[19] D.G. Hummer, K.A. Berrington, W. Eissner, A.K. Pradhan, H.E. Saraph, and J.A. Tully, Astron. Astrophys. **279**, 298 (1993).
[20] S.N. Nahar, Astrophys. J., Suppl. Ser. **101**, 423 (1995).
[21] R.L. Kelly (unpublished compilation), data were obtained from Arlene Robey of NIST.
[22] W.C. Martin, V. Kaufman, and A. Musgrove, J. Phys. Chem. Ref. Data **22**, 1179 (1993).
[23] A. Hibbert, E. Biemont, M. Godefroid, and N. Vaeck, J. Phys. B **24**, 3943 (1991).
[24] A.K. Pradhan and H.E. Saraph, J. Phys. B **10**, 3365 (1991).
[25] C. Goldbach and G. Nollez, Astron. Astrophys. **284**, 307 (1994).
[26] J.P. Doering, E.E. Gulcicek, and S.O. Vaughan, J. Geophys. Res. **90**, 5279 (1985).
[27] M. Druetta and M.C. Poulizac, Phys. Lett. **33A**, 115 (1970).
[28] C.C. Lin, D.J.G. Irwin, J.A. Kernahan, A.E. Livingston, and E.H. Pinnington, Can. J. Phys. **50**, 2496 (1972).
[29] N.H. Brooks, D. Rohrlich, and W.H. Smith, Astrophys. J. **214**, 328 (1977).
[30] J.A. Kernahan and F.R. Simpson, Nucl. Instrum. Methods Phys. Res. **202**, 49 (1982).
[31] G.M. Lawrence, Phys. Rev. A **2**, 397 (1970).
[32] W.K. Bischel, B.E. Perry, and D.R. Crosley, Chem. Phys. Lett. **82**, 85 (1981).
[33] I. Martinson, H.G. Berry, W.S. Bickel, and H. Oona, J. Opt. Soc. Am. **61**, 519 (1971).
[34] E.H. Pinnington, D.J.G. Irwin, A.E. Livingston, and J.A. Kernahan, Can. J. Phys. **52**, 1961 (1974).
[35] W.H. Smith, J. Bromander, L.J. Curtis, H.G. Berry, and R. Buchta, Astrophys. J. **165**, 217 (1971).

[36] J. Bromander, N. Duric, P. Erman, and M. Larsson, Phys. Scr. **17**, 119 (1978).
[37] *Atomic Transition Probabilities of Carbon, Nitrogen, and Oxygen, A Critical Data Compilation*, edited by W.L. Wiese, J.R. Fuhr, and T.M. Deters, J. Phys. Chem. Ref. Data Monogr. No. 7, (American Chemical Society, Washington, DC, 1996).
[38] G.C. Angel and J.A.R. Samson, Phys. Rev. A **38**, 5578 (1988).
[39] R.L. Day, R.J. Anderson, and G.J. Salamo, J. Opt. Soc. Am. **71**, 851 (1981).
[40] S. Kroll, H. Lundberg, A. Persson, and S. Svanberg, Phys. Rev. Lett. **55**, 284 (1985).
[41] J.A. Kernahan, C.C. Lin, and E.H.J. Pinnington, J. Opt. Soc. Am. **60**, 986 (1970).
[42] E.H. Pinnington, Nucl. Instrum. Methods **90**, 93 (1970).
[43] M. Druetta, M.C. Poulizac, and M. Dufay, J. Opt. Soc. Am. **61**, 515 (1971).
[44] J.H. Clark and C.E. Head, Phys. Rev. A **6**, 1722 (1972).
[45] F.J. Coetzer, T.C. Kotze, and P. van der Westhuizen, Z. Phys. A **322**, 357 (1985).
[46] J. Campbell and C.E. Head, Phys. Rev. A **13**, 1965 (1976).
[47] K.L. Bell, A. Hibbert, R.P. Stafford, and B.M. McLaughlin, Phys. Scr. **50**, 343 (1994).
[48] K.M. Aggrawal and A. Hibbert, J. Phys. B **24**, 4685 (1991).
[49] Y. Baudinet-Robinet, H-P. Garnir, P-D. Dumont, and J. Resimont, Phys. Rev. A **42**, 1080 (1990).
[50] E.H. Pinnington, K.E. Donnelly, J.A. Kernahan, and D.J.G. Irwin, Can. J. Phys. **56**, 508 (1978).
[51] D.J.G. Irwin, A.E. Livingston, and J.A. Kernahan, Nucl. Instrum. Methods **110**, 105 (1973).
[52] F.J. Coetzer, T.C. Kotze, F.J. Mostert, and P. Van der Westhuizen, Spectrochim. Acta B **41**, 847 (1986).
[53] K. Ishi, M. Suzuki, and J. Takahashi, J. Phys. Soc. Jpn. **54**, 3742 (1985).
[54] L.J. Ryan, L.A. Rayburnn, and A.J. Cunningham, J. Quant. Spectrosc. Radiat. Transf. **42**, 295 (1989).
[55] B. Denne, L. Engstrom, S. Huldt, J.O. Ekberg, L.J. Curtis, K. Ishii, E. Veje, and I. Martinson, Phys. Scr. **21**, 151 (1980).
[56] L. Engstrom, B. Denne, J.O. Ekberg, K.W. Jones, C. Jupen, U. Litzen, W.T. Meng, A. Trigueiros, and I. Martinson, Phys. Scr. **24**, 551 (1981).
[57] I.P. Buchet, M.C. Buchet-Poulizac and M. Druetta, J. Opt. Soc. Am. **66**, 842 (1976).
[58] N.M. Cann and A.J. Thakkar, Phys. Rev. A **46**, 5397 (1992).
[59] E. Trabert, P.H. Heckmann, and H.v. Buttlar, Z. Phys. A **280**, 11 (1977).
[60] J.P. Buchet, M. Dufay, and M.C. Poulizac, Phys. Lett. **40A**, 127 (1972); J.P. Buchet, M.C. Poulizac, G. Do Cao, and J. Desesquelles, Nucl. Instrum. Methods **110**, 19 (1973).
[61] H.L. Zhang, S.N. Nahar, and A.K. Pradhan (unpublished).
[62] N.S. Scott and K.T. Taylor, Comput. Phys. Commun. **25**, 347 (1982); W. Eisner (unpublished).
[63] A.K. Pradhan and H.L. Zhang, J. Phys. B **30**, L571 (1997).
[64] *Astrophysics of Gaseous Nebulae and Active Galactic Nuclei*, edited by D.E. Osterbrock (University Science Books, Sausalito, CA, 1989).
[65] S.N. Nahar, Astrophys. J. Suppl. (to be published).